

X-ray Pulses Approaching the Attosecond Frontier

Markus Drescher,^{1,2} Michael Hentschel,¹ Reinhard Kienberger,¹
Gabriel Tempea,¹ Christian Spielmann,¹ Georg A. Reider,¹
Paul B. Corkum,³ Ferenc Krausz^{1*}

Single soft-x-ray pulses of ~ 90 -electron volt (eV) photon energy are produced by high-order harmonic generation with 7-femtosecond (fs), 770-nanometer (1.6 eV) laser pulses and are characterized by photoionizing krypton in the presence of the driver laser pulse. By detecting photoelectrons ejected perpendicularly to the laser polarization, broadening of the photoelectron spectrum due to absorption and emission of laser photons is suppressed, permitting the observation of a laser-induced downshift of the energy spectrum with sub-laser-cycle resolution in a cross correlation measurement. We measure isolated x-ray pulses of 1.8 (+0.7/–1.2) fs in duration, which are shorter than the oscillation cycle of the driving laser light (2.6 fs). Our techniques for generation and measurement offer sub-femtosecond resolution over a wide range of x-ray wavelengths, paving the way to experimental attosecond science. Tracing atomic processes evolving faster than the exciting light field is within reach.

Ultrashort-pulse lasers constitute the fastest probes available for tracing transitions between different states of matter. They allow measuring time intervals on a femtosecond (1 fs = 10^{-15} s) time scale and provide access to fundamental physical, chemical, and biological processes on a microscopic scale in the time domain (1). A delayed probe pulse permits taking snapshots of atomic, molecular, or condensed-matter dynamics after excitation by a pump pulse (2). Any variation of the state of the object under study occurring during excitation by the pump or illumination by the probe remains unresolved; hence, the fastest speed at which events can be followed is limited by the laser pulse duration.

More than 30 years of evolution of ultrashort-pulse laser technology recently culminated in the generation of laser pulses shorter than 10 fs in the visible and near-infrared spectral ranges (3–9). These pulses comprise only a few oscillation cycles of the electromagnetic field and approach the ultimate limit set by the laser oscillation period $T_0 = \lambda_L/c$, where λ_L is the laser (carrier) wavelength and c is the speed of light in vacuum. Several fundamental atomic processes such as inner-shell electronic relaxation or ionization by optical tunneling, however, take place within a fraction of the oscillation period of visible or near-infrared radiation and require very short probes for being investigated. Although trains of attosecond (1 as = 10^{-18} s)

pulses at ultrahigh (T_0^{-1} or $2T_0^{-1}$) repetition rates can result from the superposition of frequency-converted coherent radiation (10–12) (most simply by superimposing on the driving field its second and third harmonic), they are of limited use for this purpose because of the very short (~ 1 to 2 fs) pulse intervals within the train. Isolated bursts of radiation on the order of 1 fs or shorter are required to reliably trace these dynamics never before accessed in the time domain. These single bursts need to be carried at substantially shorter wavelengths, preferably in the extreme ultraviolet (XUV) or x-ray regime, if bound atomic electrons are to be accessed in ultrafast spectroscopy.

High-harmonic generation (13–15) using few-cycle pulses (16–18) is ideal for this purpose. High harmonics are generated by electrons removed from the atom by the high laser field and then driven back to their ion of origin. Because their recollision energy is greatest when the laser field is largest, the most energetic “harmonic” radiation is produced at the peak of the laser pulse. We select radiation produced only within a fraction of the laser cycle near the peak of the pulse by passing the harmonics through a filter that transmits only the highest frequencies. This method has been predicted to be capable of generating single XUV/x-ray pulses of ~ 100 -as duration emitted in a collimated, laser-like beam (19–21).

Whereas the key techniques for generation have been available for several years (16, 22), methods for temporal characterization of XUV and x-ray harmonics have been restricted to bandwidths that are small compared with the laser photon energy $\hbar\omega_L$. The key to the progress reported here is a newly developed measurement technique. It allows mea-

suring the duration of broadband ($> \hbar\omega_L$) x-ray pulses with sub-laser-cycle resolution. The method is intuitive, can be generalized to a wide range of x-ray wavelengths, and offers sub-femtosecond resolution. Using this technique, we set an upper limit of 2.5 fs on the duration of isolated 90-eV x-ray pulses by our 7-fs laser-driven high-harmonic source.

Temporal characterization of high-order laser harmonics. There are currently two general approaches to pulse characterization being investigated. One aims to extend autocorrelation, developed for measuring visible pulses, into the x-ray region. Autocorrelation requires that the pulse is split into two replica pulses and then recombined in a nonlinear medium where the nonlinear process is sensitive to their temporal overlap. Unfortunately, except at the longest wavelengths (23), the XUV/x-ray pulses generated by high harmonics are currently too weak to induce measurable nonlinearities of atomic media. Thus, although autocorrelation is conceptually simple and well understood, so far it has been impossible to implement in the x-ray regime. Recently, Papadogiannis and co-workers (24) proposed an interesting variation of this concept by splitting the driving pulse rather than the harmonic pulse. The idea is that the ionizing gas, which produces the harmonics, can also be used as the nonlinear medium to measure their duration (25). They observed attosecond sub-structures on a much longer (> 10 fs) autocorrelation feature. However, although this approach is experimentally simple, it is conceptually complex because production and measurement are intertwined (26).

Our approach falls within a second class of experiments that began with the work of Schins and co-workers (27–31). Here the x-ray pulse is “cross correlated” against a short visible pulse. An x-ray photon excites a bound atomic electron into a positive-energy state in the presence of a laser field. Laser-induced transitions from this state or a laser-induced shift in its energy (Stark shift) provide the nonlinearity linking the x-ray to the laser pulse, enabling us to compare the x-ray pulse duration with that of the visible pulse. In the experiments reported so far (27–31), a number of laser photons increasing rapidly with the laser intensity are absorbed and emitted by the freed electron (forced to oscillate at ω_L). To identify the Stark shift amidst the resulting sidebands in the photoelectron energy spectrum or to measure the amplitude of the sidebands, the x-ray spectral width must be kept well below the laser photon energy $\hbar\omega_L \approx 1.6$ eV to avoid overlap of the sidebands with the main peak.

Without modification, Schins’s approach cannot be extended to sub-laser-cycle x-ray pulses for two reasons. (i) If we are to measure x-ray pulses with durations of $\tau_x < T_0$,

¹Institut für Photonik, Technische Universität Wien, Gusshausstr. 27, A-1040 Wien, Austria. ²Fakultät für Physik, Universität Bielefeld, D-33615 Bielefeld, Germany. ³National Research Council of Canada, Ottawa, Ontario, Canada K1A 0R6.

*To whom correspondence should be addressed. E-mail: ferenc.krausz@tuwien.ac.at

the photoelectron energy distribution must become broader than the laser photon energy so that it is no longer possible to identify individual sidebands and measure their amplitudes or determine the Stark shift. (ii) If the field is increased to increase the Stark shift so it becomes measurable, absorption and emission of laser photons tend to smear the photoelectron energy distribution beyond redemption.

In what follows, we show that choosing the geometry of observation carefully and confining the laser field to a few oscillation cycles opens the door to broadband ($> \hbar\omega_L$) x-ray pulse measurement with sub-femtosecond resolution.

Laser-assisted lateral x-ray photoionization. To gain insight into the role of the observation geometry, consider the laser-assisted photoelectric effect in a semi-classical analysis (32–35). The electron is set free by an x-ray photon of energy $\hbar\omega_x$ at a delay time t_d with respect to the peak of the visible laser pulse having an initial kinetic energy $W_0 = mv_i^2/2 = \hbar\omega_x - W_b$, where W_b is the ionization potential of the atom, in an arbitrary direction. For $\hbar\omega_x \gg W_b$, the strong, linearly polarized “probe” laser field $E_L(t) = E_a(t) \cos(\omega_L t + \varphi)$ is predominant in governing electron motion after ionization. In the adiabatic limit $dE_a/dt \ll E_a\omega_L$ (which is a remarkably good approximation even for our 7-fs pulses) the equation of motion can then be readily integrated, yielding the connection

$$v_{\parallel,f} = \sqrt{\frac{4U_p(t_d)}{m}} \sin(\omega_L t_d + \varphi) + v_{\parallel,i} \quad (1)$$

between the initial ($v_{\parallel,i}$) and final value ($v_{\parallel,f}$) of the velocity component parallel to the laser polarization. Here $U_p(t) = e^2 E_a^2(t)/4m\omega_L^2$, which, in the adiabatic limit, represents the cycle-averaged quiver energy of the electron (mass m and charge $-e$) and is commonly referred to as the ponderomotive energy (36). For the transverse component, $v_{\perp,f} = v_{\perp,i}$. Using these relations along with the above constraint on the initial kinetic energy, the final kinetic energy (after the laser pulse) can, in the limit of $\omega_x \gg \omega_L$, be expressed as

$$W_f \approx W_0 - U_p(t_d) + U_p(t_d) \cos 2\omega_L t_d + 4U_p(t_d) \cos^2 \theta \sin^2 \omega_L t_d + \sqrt{8W_0 U_p(t_d)} \cos \theta \sin \omega_L t_d \quad (2)$$

where θ is the angle of the final electron momentum \mathbf{p}_f with respect to the laser polarization (Fig. 1). Here, for the sake of brevity we assumed $\varphi = 0$. To account for x-ray excitation of nonzero temporal and spectral width, we expanded our simple analysis by a numerical simulation. It allows us to calculate the electron energy spectrum observed within a given range of observation angles θ . In spite of its deficiencies, however, Eq. 2

provides insight into the basic physics and leads us to the optimum design of the experiment for x-ray pulse measurement.

The second term on the right-hand side of Eq. 2 lowers the final kinetic energy of the electron by its quiver energy at the instant of its “birth.” This energy is transferred to the laser field by blue-shifting its carrier frequency for fs pulse durations (37, 38). The third to fifth terms correspond to the absorption and emission of laser photons in a quantum description. For a brief analysis, consider two limiting cases represented by an x-ray bandwidth much smaller or much greater than the laser photon energy, respectively. The former condition implies $\tau_x \gg T_0$, resulting in the appearance of discrete sidebands spaced by $\hbar\omega_L$ around the main peak in the photoelectron energy spectrum. This is the regime of previous studies (27–31). For $W_0 \gg U_p$, the overall width of the sideband spectrum can be evaluated from Eq. 2 as $2\sqrt{8W_0 U_p(t_d)} \cos \theta$, and its center of gravity is upshifted by $2U_p(t_d) \cos^2 \theta$ with respect to $W_0 - U_p(t_d)$ (the position of the main peak) due to a higher amplitude of Stokes (photon absorption) as compared with anti-Stokes sidebands (photon emission). In this limit, both the ponderomotive shift $U_p(t_d)$ and the amplitude of sidebands can be accurately measured.

In the opposite limit, for an x-ray spectral width larger than $\hbar\omega_L$, the sidebands completely coalesce (due to a distribution of W_0 over a range broader than $\pm \hbar\omega_L$), forming a single broad spectral feature with a width and center-of-gravity position as given above. Consequently, neither the individual sideband amplitudes nor the ponderomotive shift can be reliably acquired from the photoelectron spectrum any longer. The ponderomotive shift tends to be fully obscured by an upshift in the center-of-gravity of the overall spectral feature (fourth term in Eq. 2). This upshift means a net absorption of laser photons and is most pronounced for $\theta \approx 0$.

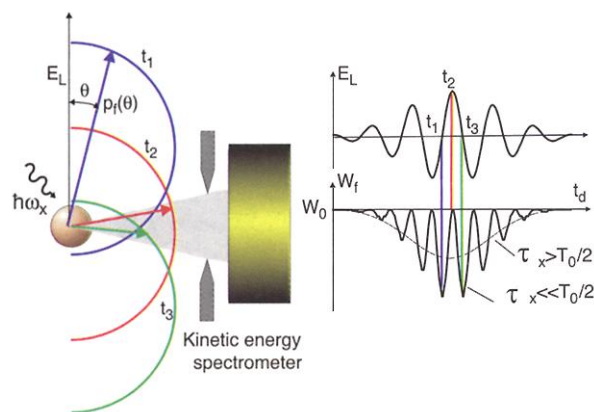
Moreover, $\hbar\omega_x \gg W_b > U_p$ implies $\sqrt{8W_0 U_p} \gg U_p$, i.e., the photoelectron energy spectrum is “smeared out” over an energy range much broader than U_p , impeding a reliable measurement of its shift of the order of $U_p(t_d)$. Electrons ejected at $\theta \approx 90^\circ$ are special in that their energy spectrum is hardly distorted by the absorption and emission of laser photons, but is just shifted by the oscillating laser field. This central finding from our simple analysis is the basis for our broadband x-ray pulse measurement.

Choosing the observation angle as $\theta \approx 90^\circ$ (orthogonal to the laser polarization) eliminates the last two terms in Eq. 2 and thereby makes the ponderomotive shift $-U_p(t_d)$ clearly observable. Because $U_p(t) \propto E_a^2(t)$, measurement of the ponderomotive shift as a function of the delay t_d yields a cross correlation between the temporal intensity profiles of the x-ray and laser pulses. The predicted oscillations in the electron energy shift (third term in Eq. 2) offer a sub- $T_0/4$ probe for measuring x-ray emission characteristics on an attosecond time scale, reminiscent of the concept of an optically driven streak camera (25, 39). These oscillations average out for $\tau_x \geq T_0/2$.

Intuitively, the simplified dynamics (oscillating downshift) can be understood as an impact of the laser field on the electron momentum distribution (Fig. 1). The final x-ray photoelectron momentum distribution $\mathbf{p}_f(\theta)$ gets shifted along the laser polarization, owing to a momentum transfer that reverses its sign twice within a laser oscillation period. This momentum transfer translates into a downshift in W_f for detection angles near $\theta = 90^\circ$, oscillating at $2\omega_L$ with its envelope following $U_p(t_d)$, i.e., the temporal intensity profile of the laser pulse.

In this observation geometry (Fig. 1), we confine detection to a small solid angle around $\theta = 90^\circ$ instead of collecting all electrons ejected in 2π (or 4π), as has been

Fig. 1. Semiclassical modeling of laser-assisted x-ray photoionization. The electrons set free at different instants (t_1, t_2, t_3) by an x-ray photon are ejected with different angle distributions of their final momenta $\mathbf{p}_f(\theta)$ in the presence of a laser field. The momentum transferred along the laser polarization translates into a downshift of the kinetic energy W_f of the electrons observed (within a small solid angle) orthogonally to the laser polarization. The variation of W_f with the time delay between the instant of x-ray absorption and the peak of the laser pulse (assuming an x-ray pulse duration $\tau_x \ll T_0/2$ and observation near $\theta = 90^\circ$) exhibits a modulation at twice the laser frequency with an envelope following the temporal evolution of the laser intensity. For $\tau_x > T_0/2$, the oscillations average out (dashed line).



the case in all relevant experiments so far (27–31). In addition to the benefits discussed above, this geometry also helps suppress undesirable background resulting from electrons produced by multiphoton above-threshold ionization (ATI) by the laser field alone. Other than the particular observation geometry, confinement of the interaction to a few-laser oscillation cycles is important (i) for enhancing the ponderomotive downshift at low levels of ATI background and (ii) for a steep temporal intensity gradient, yielding a high “streaking” speed for measuring x-ray transients down to the 1-fs range, where the sub- $T_0/4$ probe (see third term in Eq. 2) comes into play.

Apparatus for laser harmonic generation and measurement. To exploit the potential of the above described technique for measuring x-ray bursts with high temporal resolution, jitter between the x-ray pulse and the laser pulse probing the x-rays needs to be minimized. This requirement can be most efficiently fulfilled by using the same laser pulse for generation and measurement, which becomes feasible because of the low levels of ionization at which few-cycle drivers are able to efficiently generate harmonics up to the 100-eV region (40). As a result, an enhanced conversion efficiency is combined with a nearly undistorted propagation of the laser pulse through the weakly ionizing harmonic source. This enables us to record high-resolution cross-correlations with the co-propagating, perfectly synchronized harmonic pulse by using a compact, highly stable delay stage.

We focus laser pulses carried at $\lambda_L \approx 770$ nm ($\hbar\omega_L \approx 1.6$ eV) with a duration of 7 fs and pulse energy of 0.5 mJ delivered at a repetition rate of 1 kHz (22) into a quasi-static neon gas cell (Fig. 2). Harmonics in the same geometry and under similar experimental conditions as described in (40) are produced up to photon energies of ~ 120 eV with a divergence angle of ~ 0.7 mrad in the near-cutoff region. The co-propagating x-ray and laser pulses are passed through a pellicle with a central circular zone formed by a zirconium foil that is transparent for the x-rays but blocks laser radiation. The resulting annular laser beam and the concentric harmonic beam hit a Mo/Si spherical multilayer mirror ($R_{\text{peak}} \approx 60\%$ at 90 eV, bandwidth ≈ 5 eV) consisting of two piezo-controlled concentric parts. The two-component mirror forms a compact, virtually jitter-free delay stage for the laser and the harmonic pulses with a maximum scan range of ~ 50 fs and a resolution and reproducibility of better than 0.1 fs. The folding angle is kept below 5° to minimize astigmatism. Spherical aberration gives rise to a time smearing of < 0.05 fs for the harmonic and < 1 fs for the laser beam. The harmonics are focused to a diameter of ~ 2 μm (41), which is small compared with the ~ 20 - μm diameter of the focused laser beam, ensuring a nearly constant laser intensity in the interaction volume. The target atoms effuse from a 100- μm -long, 20- μm -wide slit aligned parallel to the propagation direction of the beams. The entrance of a 0.4-m

time-of-flight (TOF) photoelectron spectrometer (resolution ≈ 0.5 eV at 75 eV) with an acceptance angle of 0.3 sr is brought in close proximity (5 mm) to the interaction volume. The spectrometer axis is aligned perpendicularly to the laser beam direction and to the laser polarization ($\theta = 90^\circ$).

X-ray/laser-pulse cross correlation in the few-cycle regime. The lowest plot (full line) in Fig. 3 depicts the 4p-photoelectron energy spectrum of krypton obtained in the absence of the laser field. Krypton has been chosen as a target because of the nearly isotropic momentum distribution of 4p electrons at $\hbar\omega_x \approx 90$ eV photon energy (42, 43). The shape of the 4p spectrum is determined by the high-harmonic spectrum after reflection off the Mo/Si multilayer (the dashed line showing the spectral reflectance shifted by the ionization potential $W_b = 14.0$ eV of Kr). The mirror reflects harmonics H55 and H57, which can be barely discriminated due to their coalescence. Assuming no spectral phase modulation, Fourier transformation of the spectrum yields a pulse duration of 0.4 fs (full width at intensity half maximum).

To measure the x-ray pulse duration, we performed x-ray photoionization experiments in the presence of the few-cycle laser field. The laser intensity was adjusted to result in a maximum ponderomotive energy of $U_p \approx 2$ eV, ensuring negligible ATI for our pulse duration. Figure 3 depicts x-ray

Fig. 2. Schematic diagram of the experimental setup. The focused 7-fs laser beam fights its way through the walls of a metallic tube (diameter ≈ 3 mm) by ablation and interacts with neon atoms inside the tube to produce high-harmonic radiation. The ionizing neon gas streaming out of the tube can be traced because of its fluorescence emission (see photograph). The laser and the highly collimated x-ray beam emerging from the interaction region within the tube co-propagate collinearly (along the axis of the emission cone) through a 2-m beamline toward the measurement. Differential pumping stages reduce the pressure from $\sim 4 \times 10^{-2}$ mbar in the source chamber to the range of $\sim 10^{-5}$ mbar in the experimental chamber. An ionization detector in the higher-pressure part of the beamline serves for monitoring the spectrally integrated high-harmonic flux. In the beamline, the laser and harmonic beams pass through a 200-nm-thick, 3-mm-diameter zirconium foil placed on a 5- μm -thick nitrocellulose pellicle to cover a hole of 2-mm diameter. The energy transported by the resulting annular laser beam can be adjusted with a motorized iris between a fraction of a microjoule and a few tens of microjoules. The Mo/Si multilayer consists of an annular part that has an outer diameter of 10 mm with a concentric hole of 3-mm diameter hosting a miniature mirror of slightly smaller diameter. Both parts originate from the same substrate, ensuring identical radii of curvature ($R = 70$ mm). The miniature central mirror is mounted on a quadrant piezo stage (PZT), allowing alignment and translation with respect to the external part.

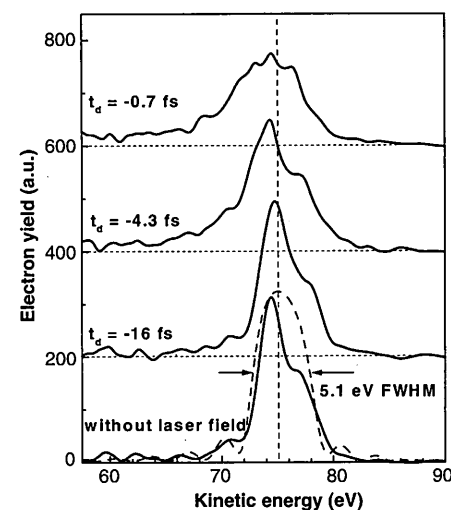
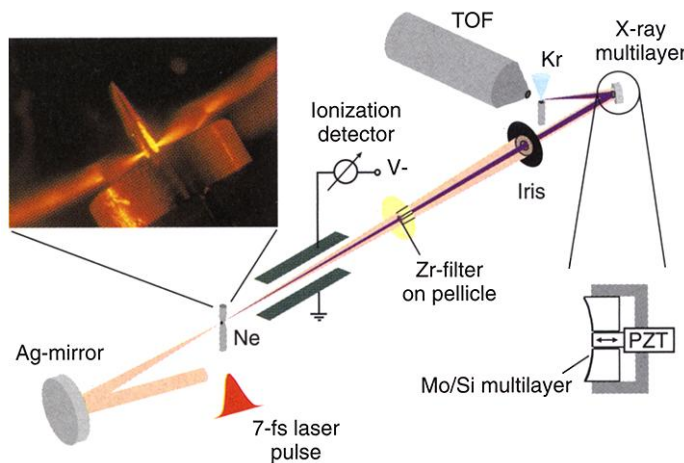


Fig. 3. X-ray photoelectron spectra produced by 90-eV harmonics of 7-fs laser pulses in Kr in the presence of the laser field for different delays t_d of the x-ray pulse with respect to the laser pulse. The laser peak intensity at target is calculated from the maximum ponderomotive shift as $\sim 4 \times 10^{13}$ W/cm². The spectra were recorded over an acquisition period of 200 s by collecting ~ 1500 signal counts with a minor background from ATI electrons, which were subtracted. The dashed line depicts the reflectivity (peak $\approx 60\%$, bandwidth ≈ 5.1 eV) of the Mo/Si multilayer shifted by the ionization potential.

photoelectron spectra recorded at various delays t_d of the x-ray pulse with respect to the laser pulse. Comparison of the spectra recorded in the absence of the laser field and for $t_d = -16$ fs (no temporal overlap) shows little influence of space-charge effects by ATI electrons.

A contour plot (Fig. 4) illustrates the evolution of the 4p spectrum of Kr for increasing delay of the x-ray pulse (recorded from $t_d = -16$ fs to $t_d = 25.3$ fs in 27 steps). In spite of the high laser peak intensity, the x-ray photoelectron spectrum remains “intact” throughout the region of temporal overlap between the laser pulse and the x-ray pulse. Eq. 2 reveals that this is a direct consequence of our specific observation geometry. Under our experimental conditions, the photoelectron spectrum would be broadened to cover a range of $2\sqrt{8W_0}U_p(t_d = 0) \approx 60$ eV in a 2π (or 4π) detection geometry (27–31). By contrast, in our lateral ($\theta \approx 90^\circ$) observation geometry the effective broadening amounts to merely a few eV (caused by the finite detection solid angle). As a result, a downshift on the order of $U_p \approx 2$ eV is clearly discernible. A notable shift of the center of gravity is confined to a delay range of less than 10 fs and accompanied by some (asymmetric) broadening. This becomes evident from the white iso-spectral-density lines or from a comparison of the broadened spectra recorded at the slope ($t_d = -4.3$ fs) and at the peak ($t_d = -0.7$ fs), respectively, with a spectrum well before the arrival of the laser pulse ($t_d = -16$ fs) in Fig. 3. These observations are in excellent agreement with simulations based on our semiclassical model and performed for finite x-ray pulse duration and bandwidth.

X-ray pulses with sub-laser-cycle duration. For a quantitative analysis, we evaluated the first-order moments (center of gravity) of the measured photoelectron spectra as a function of t_d (Fig. 5). Accord-

ing to Eq. 2, the center-of-gravity shift with varying delay t_d displays directly the evolution of the ponderomotive energy U_p during the laser pulse. Assuming the laser pulse as bandwidth-limited at the entrance of the high-harmonic target, we simulated the propagation of the 7-fs pulses with an initial peak intensity of 7×10^{14} W/cm² through the neon target (44). The initial pulse shape is obtained by inverse Fourier-transformation from the measured pulse spectrum. The ionizing target becomes somewhat dispersive for the peak and trailing edge of the pulse, resulting in a pulse-broadening to ~ 7.5 fs. However, because ionization is virtually confined to a single cycle near the pulse peak, the leading edge is hardly affected by dispersion in the harmonic source, constituting a steep probe (rise time $\tau_r \approx 5$ fs) for the x-ray temporal intensity profile.

The laser “probe” obtained from this numerical analysis is idealized in that it has a rise time τ_r equal to its theoretical limit. To obtain a conservative upper limit on the x-ray pulse duration, we first convolve this idealized probe with a hypothetical x-ray pulse obtained by inverse Fourier transformation of the lowest spectrum shown in Fig. 3, allowing for an adjustable quadratic spectral phase (as a fit parameter) that determines the x-ray pulse duration τ_x . The solid line in Fig. 5 represents the best fit to the measured data, obtained from a convolution of a 2.4-fs x-ray pulse with the idealized probe. For a realistic rise time of the laser pulse front increased by $\delta\tau_r$, this value is to be corrected by $\delta\tau_x \approx -(\tau_r/\tau_x)\delta\tau_r$. With a conservative estimate of $\delta\tau_r \geq 0.3$ fs from inspection of the most prominent pulse-broadening effects (spherical aberration and nonlinear spectral phase) and an F-stat goodness-of-fit analysis of the cross-correlation (Fig. 5), we obtain $\tau_x = 1.8$ (+0.7/–1.2) fs full width at intensity half maximum (FWHM) (45).

This result has been corroborated by tracing the evolution of the low-energy electron yield as a function of the delay t_d between the x-ray pulse and the laser pulse. Numerical simulations based on our semi-classical analysis of laser-assisted x-ray photoionization predict this signal to be “switched on” somewhat faster than the rise time of the front edge of the laser pulse because of a finite threshold intensity needed for the production of these electrons. The shorter rise time offers a probe with enhanced resolution for x-ray pulse measurements. The evaluation of the electron yield (Fig. 6) with $W_f \leq 71$ eV as a function of t_d by fitting an error function to the data results in rise times of 3.1 ± 0.6 fs and 2.9 ± 0.5 fs, respectively. The error-function fit is consistent with a Gaussian-like x-ray pulse profile and a steep probe function with a rise time comparable to or shorter than the pulse duration. Deconvolution yields an upper limit of ~ 2 fs on the x-ray pulse duration, in fair agreement with the above result.

Current limitations and future challenges. There are several predictions suggesting that isolated XUV/x-ray pulses in the range of 100 as can be generated (18–21, 46). However, before these pulses become available for experiments, a few problems need solving.

First, we need a reliable and simple method of measuring the temporal structure of broadband x-ray emission with a resolution of approximately 0.1 fs. We believe that the technique introduced in this paper is capable of solving this problem with the sub- $T_0/4$ probes that originate from the predicted oscillations in the electron energy shift (Fig. 1, Eq. 2). However, both the measurement (47)

Fig. 4. Contour plot of the evolution of the 4p spectrum of Kr comprising 28 spectra recorded within the depicted range of delay time between the x-ray and laser pulse. Blue, low-spectral electron density; red, high-spectral electron density; white, iso-spectral-density lines. Typically, 1000 to 1500 counts contributed to the spectra, which were renormalized to a constant area for the contour diagram. It took approximately 2 hours to acquire the data used for this plot. For delays $t_d > 5$ fs, a gradual spectral redistribution of x-ray energy in favor of H57 occurs due to laser energy drift-induced minor shift in the harmonic peak positions with respect to the (steep) edges of the Mo/Si mirror reflectance curve (Fig. 3). This is caused by a drift of the laser pulse energy as small as a few percent, which can not be avoided on a time scale of hours.

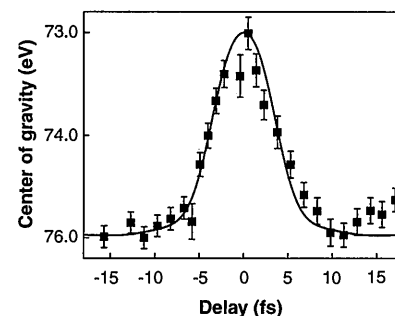
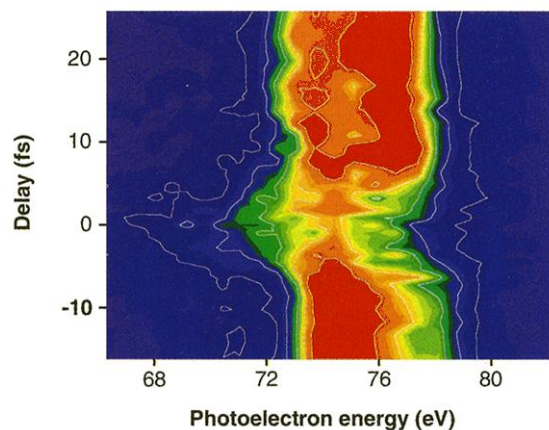


Fig. 5. Center of gravity of the measured Kr 4p spectra (squares) as a function of the x-ray pulse delay. Line corresponds to the intensity envelope correlation function of the 90-eV x-ray pulse and the driving laser pulse, best fit to the leading edge (-10 fs $\leq t_d \leq 0$) data obtained with an x-ray pulse of $\tau_x = 2.4$ fs in duration. The intensity envelope of the laser pulse was computed assuming the absence of pulse-broadening effects other than dispersion introduced by the ionizing harmonic source. The observed post-pulsing is a consequence of a small residual spectral phase carried by the initial laser pulse (54), which is neglected in our modeling.

and the generation (48) technique demonstrated here need to be improved to permit reliable attosecond metrology. Lastly, improved characterization and control of strong laser pulses is required for achieving this objective. Because attosecond pulses are generated by sub-period dynamics from a visible pulse, the optical pulse field must be controlled on a sub-period scale. That is, we require the optical oscillations to fit reproducibly (with attosecond precision) within the pulse envelope for the generation of single attosecond pulses with reproducible amplitude and timing. Technically, the carrier-envelope phase [denoted by φ in the expression of $E_L(t)$] must be controlled, or at least known. Carrier-envelope phase control (49–51) with sub-cycle precision (52) has been demonstrated for low-energy pulse trains. Amplification of these pulses with low jitter of φ and subsequent accurate single-shot measurement of φ for the intense laser pulses (53) is another prerequisite for the development of attosecond metrology.

In conclusion, we believe that the experimental techniques are now available for measuring sub-light-cycle dynamics. The single attosecond x-ray pulses that will be generated will open a new chapter in ultrafast spectroscopy. Just as femtosecond pulses allow the observation of the motion of atoms in molecules, attosecond pulses will allow us to trace electronic motion and electronic relaxation (such as inner-shell dynamics) in atoms and molecules. In addition, attosecond science will have strong, phased laser fields perfectly synchronized with the attosecond pulse. The laser fields will be strong enough and well-enough controlled to govern electron dynamics (in fact, this is how high harmonics are produced), and well-enough synchronized to attosecond pulses to allow sub-laser-cycle measurements. Studying strong-field electron dynamics (such as optical-field

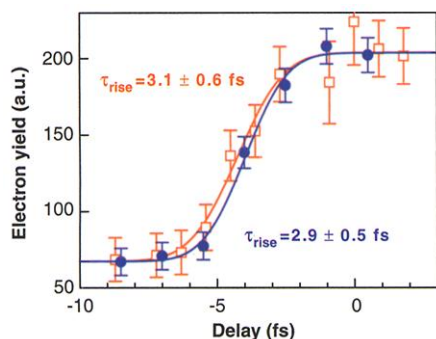


Fig. 6. Electron yield at the low-energy tail of the 4p spectrum obtained on different days and under slightly different conditions within the energy interval of 68 to 71 eV (open squares) and of 64 to 71 eV (solid circles) versus delay time t_d between x-ray and laser pulse. The corresponding lines represent error-function fits to the measured data, yielding a rise time of 3.1 ± 0.6 fs and 2.9 ± 0.5 fs, respectively.

ionization) and controlling these processes will be a forefront of attosecond science.

References and Notes

- J.-C. Diels, W. Rudolph, *Ultrashort Laser Pulse Phenomena* (Academic Press, New York, 1996).
- Fast heavy-ion impact can trigger atomic processes (e.g., ionization) on an unprecedented, attosecond time scale as demonstrated by R. Moshhammer *et al.* [*Phys. Rev. Lett.* **79**, 3621 (1997)]. However, the lack of a synchronized probe pulse of comparable duration does not allow tracing of dynamics after the impact.
- A. Baltuska *et al.*, *Appl. Phys. B* **65**, 175 (1997).
- M. Nisoli *et al.*, *Appl. Phys. B* **65**, 189 (1997).
- U. Morgner *et al.*, *Opt. Lett.* **24**, 411 (1999).
- D. H. Sutter *et al.*, *Opt. Lett.* **24**, 631 (1999).
- A. Shirakawa *et al.*, *Appl. Phys. Lett.* **74**, 2268 (1999).
- G. Steinmeyer *et al.*, *Science* **286**, 1507 (1999).
- T. Brabec, F. Krausz, *Rev. Mod. Phys.* **72**, 545 (2000).
- T. W. Hänsch, *Opt. Commun.* **80**, 71 (1990).
- G. Farkas, C. Toth, *Phys. Lett. A* **168**, 447 (1992).
- S. E. Harris *et al.*, *Opt. Commun.* **100**, 487 (1993).
- A. L'Huillier, Ph. Balcou, *Phys. Rev. Lett.* **70**, 774 (1993).
- J. J. Macklin, J. D. Kmetec, C. L. Gordon III, *Phys. Rev. Lett.* **70**, 766 (1993).
- M. Lewenstein *et al.*, *Phys. Rev. A* **49**, 2117 (1994).
- Ch. Spielmann *et al.*, *Science* **278**, 661 (1997).
- M. Schnürer *et al.*, *Phys. Rev. Lett.* **80**, 3236 (1998).
- Ch. Spielmann *et al.*, *IEEE J. Sel. Top. Quantum Electr.* **4**, 249 (1998).
- K. J. Schafer, K. C. Kulander, *Phys. Rev. Lett.* **78**, 638 (1997).
- I. P. Christov, M. M. Murnane, H. C. Kapteyn, *Phys. Rev. Lett.* **78**, 1251 (1997).
- C. Kan *et al.*, *Phys. Rev. Lett.* **79**, 2971 (1997).
- S. Sartania *et al.*, *Opt. Lett.* **22**, 1562 (1997).
- Y. Kobayashi *et al.*, *Opt. Lett.* **23**, 64 (1998).
- N. A. Papadogiannis *et al.*, *Phys. Rev. Lett.* **83**, 4289 (1999).
- E. Constant *et al.*, *Phys. Rev. A* **56**, 3870 (1997).
- The signal detected by Papadogiannis *et al.* (24) can be regarded as a high-order autocorrelation of the driver laser pulse. The extent to which this provides insight into the temporal structure of the generated high harmonics (autocorrelation signal) is not quite clear at present.
- J. M. Schins *et al.*, *Phys. Rev. Lett.* **73**, 2180 (1994).
- J. M. Schins *et al.*, *J. Opt. Soc. Am. B* **13**, 197 (1996).
- T. E. Glover *et al.*, *Phys. Rev. Lett.* **76**, 2468 (1996).
- A. Bouhal *et al.*, *J. Opt. Soc. Am. B* **14**, 950 (1997).
- E. S. Toma *et al.*, *Phys. Rev. A* **62**, 061801(R) (2000).
- T. F. Gallagher, *Phys. Rev. Lett.* **61**, 2304 (1988).
- H. B. van Linden van den Heuvel, H. G. Muller, in *Multiphoton Processes*, S. J. Smith, P. L. Knight, Eds. (Cambridge Univ. Press, Cambridge, 1988), pp. 26–44.
- P. B. Corkum, N. H. Burnett, F. Brunel, *Phys. Rev. Lett.* **62**, 1259 (1989).
- P. B. Corkum, *Phys. Rev. Lett.* **71**, 1994 (1993).
- Note that within the adiabatic approximation, the cycle-averaged quiver energy is a meaningful physical quantity even if $\tau_x \ll T_0$ because the velocity and, hence, the kinetic energy can be unambiguously decomposed into a quiver (U_p) and drift component.
- R. R. Freeman *et al.*, *Phys. Rev. Lett.* **59**, 1092 (1987).
- E. Yablonovitch, *Phys. Rev. Lett.* **60**, 795 (1988).
- A. Scrinzi, M. Geissler, T. Brabec, *Phys. Rev. Lett.* **86**, 412 (2001).
- M. Schnürer *et al.*, *Phys. Rev. Lett.* **83**, 722 (1999).
- M. Schnürer *et al.*, *Appl. Phys. B* **70**, S227 (2000).
- U. Becker, D. A. Shirley, *VUV and Soft X-Ray Photoionization* (Plenum, New York, 1996), p. 152.
- The photoelectrons originating from the 4s level (kinetic energy ≈ 62 eV) are suppressed in this geometry due to their anisotropic momentum distribution, (42).
- Laser pulse propagation and generation of high-order harmonics in our neon target were modeled from the quantum theory of M. Lewenstein *et al.* (15), expanded to account for nonadiabatic effects, ground-state depletion, and the influence of the atomic Coulomb field on ionization (9) and from Maxwell's wave equation. The latter also includes the refractive index of the neutral atoms and the absorption coefficient at high-harmonic frequencies (40). The laser and target parameters used are as follows: input laser pulse shape, as calculated from the measured spectrum; initial duration, 7 fs; target length, 2.5 mm; and pressure, 200 mbar.
- Due to a sensitivity of τ_x to minor changes in τ , our error propagation analysis yields a lower boundary of the confidence interval of τ_x that is inconsistent with the measured x-ray spectrum (Fig. 3). Therefore, the lower boundary has been replaced by the limit obtained from our numerical analysis (44), $\tau_{x,\min} \approx 0.6$ fs.
- P. B. Corkum, N. H. Burnett, M. Yu. Ivanov, *Opt. Lett.* **19**, 1870 (1994).
- Our simulations indicate that exploitation of the attosecond potential of our measurement technique calls for smaller solid angles of detection than used in our experiments. In our attempts to resolve sub-femtosecond x-ray emission structure, we have been able to observe first indications of the predicted oscillations (third term in Eq. 2) over a delay range of several laser cycles near $t_d \approx 0$. Currently, however, the signal-to-noise ratio is strongly compromised by the reduced solid angle of detection. Somewhat higher harmonic photon yields appear to be necessary for performing attosecond-resolution measurements.
- To provide more x-ray photons for measurement and to shorten the x-ray pulses, the generation process needs to be improved. Our simulations (44) confirm the sub-laser-cycle duration of the 90-eV harmonic emission for the parameters used in our experiments but indicate a sensitive dependence of its "sub-structure" on the laser peak intensity I_p . The ability to keep I_p at $\sim 5 \times 10^{14}$ W/cm² across the entire interaction volume would allow us to confine 90-eV harmonic emission to a fraction of a half cycle near the pulse peak, with $\tau_x \approx 0.6$ fs (limited by the Mo/Si mirror bandwidth). However, an increase of I_p to $\sim 7 \times 10^{14}$ W/cm² at the center of our Gaussian beam profile is predicted to give rise to a double-peaked emission of ~ 2 -fs duration for near-axis rays. Reducing the on-axis intensity to $\sim 5 \times 10^{14}$ W/cm² would remove this broadening, but only at the (currently unacceptable) expense of 90-eV photon yield (due to a lateral confinement of the emission volume). Moreover, increasing the bandwidth of the multilayer for supporting shorter x-ray pulses tends to further compromise the photon flux on target. Increasing the power of few-cycle driven x-ray harmonic sources and/or developing techniques for efficient conversion of a Gaussian into a flat-top beam profile, therefore, will be of central importance for pushing the limits of the demonstrated techniques for generation and measurement into the 100-as range.
- L. Xu *et al.*, *Opt. Lett.* **21**, 2008 (1996).
- D. J. Jones *et al.*, *Science* **288**, 635 (2000).
- A. Apolonski *et al.*, *Phys. Rev. Lett.* **85**, 740 (2000).
- A. Poppe *et al.*, *Appl. Phys. B* **72**, 373 (2001). Published online 13 December 2000; 10.1007/S003400000526.
- P. Dietrich, F. Krausz, P. B. Corkum, *Opt. Lett.* **25**, 16 (2000).
- Z. Cheng *et al.*, *Opt. Lett.* **24**, 247 (1999).
- U. Heinzmann from the University of Bielefeld and his colleagues, U. Kleineberg and Y. Lim, provided invaluable x-ray optical components and support for the experiments. The Zr filters were provided by G. Schmaßl from the University of Göttingen. The computer code used for simulating high-harmonic generation was developed under the guidance of T. Brabec. All contributions are gratefully acknowledged. Sponsored by the Austrian Science Fund (grants Y44-PHY and F016) of the Federal Ministry of Education, Science, and Culture; M.D. acknowledges a fellowship in the frame of the European ATTO network and support from the Ministry of Education, Science and Research NRW.

22 December 2000; accepted 2 February 2001
Published online 15 February 2001;
10.1126/science.1058561
Include this information when citing this paper.